Supplementary Material

Light-induced vacuum micromotors based on an antimony telluride microplate

Weiwei Tang[a,b,c,*], Qiannan Jia[b,c], Yong Wang[b,c], Ding Zhao[b,c], Wei Lyu[b,c], Wei Yan[b,c,*], and Min Qiu[b,c,*]

[a]University of Chinese Academy of Sciences, Hangzhou Institute for Advanced Study, College of Physics and Optoelectronic Engineering, Hangzhou, China

[b]Westlake University, School of Engineering, Key Laboratory of 3D Micro/Nano Fabrication and Characterization of Zhejiang Province, Hangzhou, China

[c]Institute of Advanced Technology, Westlake Institute for Advanced Study, Hangzhou, China

The PDF file includes:

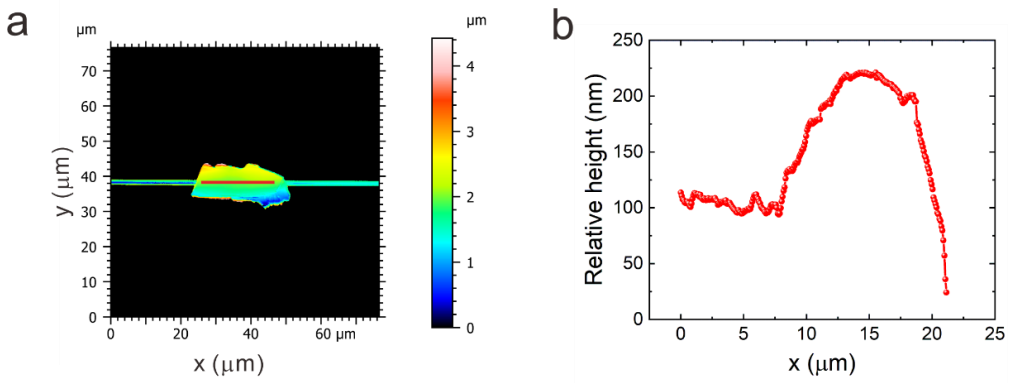

Fig. S1. The surface morphology of the Sb_2Te_3 plate on a silica microfiber. (a) Confocal laser scanning microscopy (CLSM) image of the Sb_2Te_3 plate on a silica microfiber. (b) Height profile taken from the CLSM image along a selected line [red solid line in (a)]. The fluctuation in surface height is up to 200 nm, implying that the surface of the plate is curved.

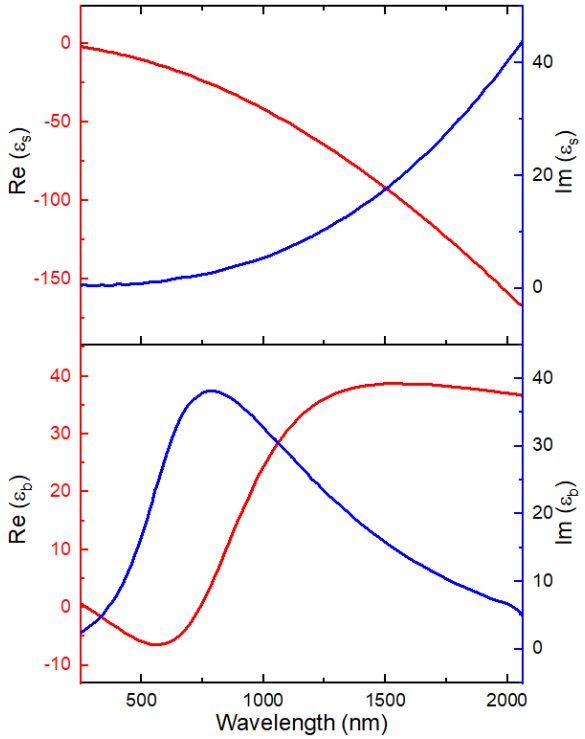

Fig. S2. Permittivity of metallic surface layer (upper panel) and insulating bulk (low panel) of Sb_2Te_3 [29]. The surface layer is set to be 2.6 nm.

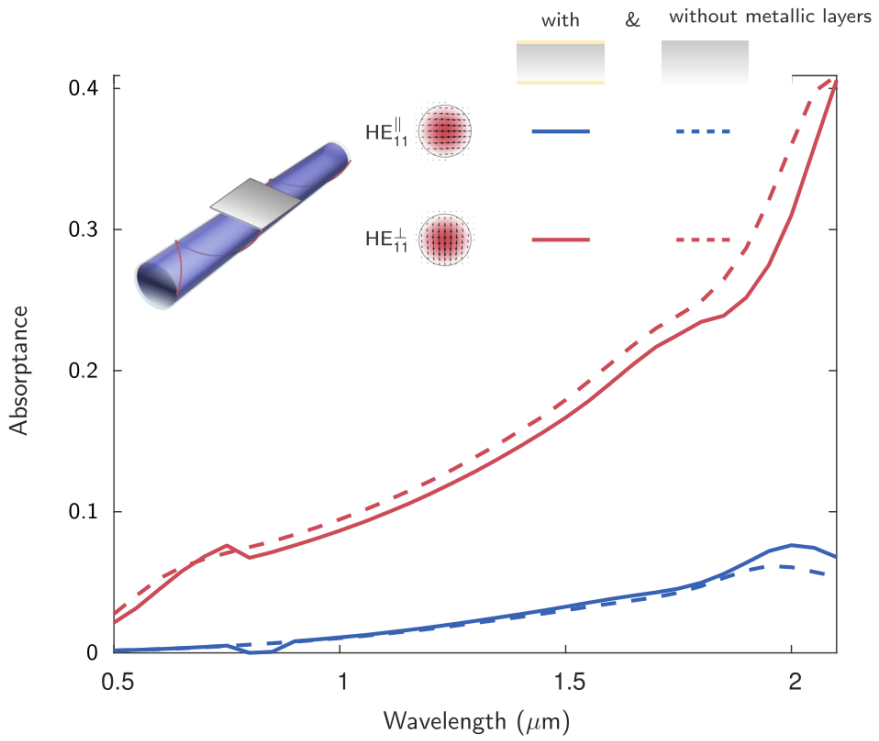

Fig. S3. Absorption spectrum of a Sb_2Te_3 plate on a microfiber. The structure has the same geometrical parameters as Fig. 1(c)-(e) in the system. Fundamental modes $HE_{11}^{\parallel}$ and $HE_{11}^{\perp}$ supported by the microfiber are taken as incident waves. Two cases including and excluding 2.6-nm metallic layers in the Sb_2Te_3 plate are compared.

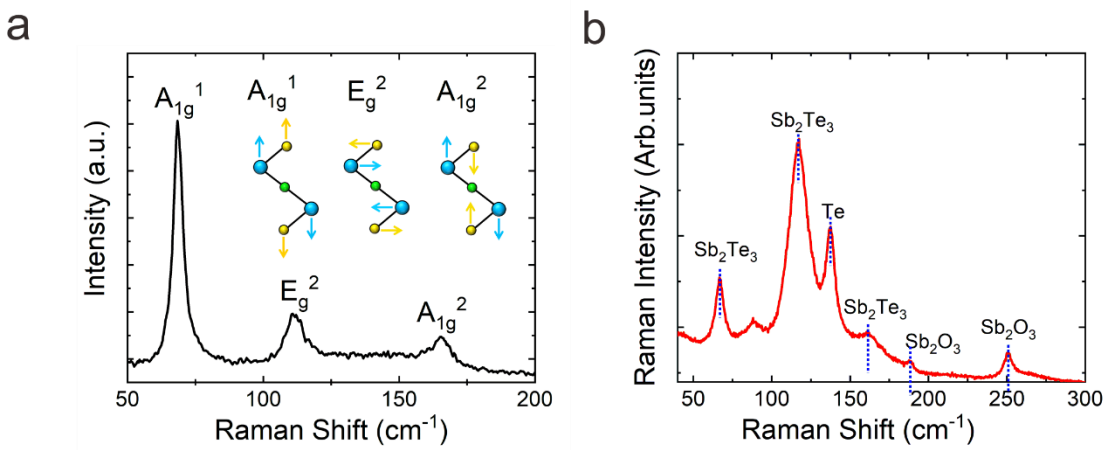

Fig. S4. Micro-Raman spectrum of a Sb_2Te_3 plate before (a) and (b) after nanosecond laser illumination. Before the nanosecond laser illumination, three characteristic peaks at 68.26 cm^{-1}, 112.45 cm^{-1}, 165.36 cm^{-1} of Sb_2Te_3 are observed, corresponding to A_{1g}^1, E_g^2, and A_{1g}^2 phonon vibrational modes, respectively. After the nanosecond laser illumination, in addition to three previous peaks, three new characteristic peaks centered at 137.6 cm^{-1}, 188.3 cm^{-1}, 250.8 cm^{-1} are observed. The new peaks are attributed to Raman active mode of trigonal Te [35] and cubic Sb_2O_3 [36]. The oxygen element in Sb_2O_3 might be from oxidation of Sb at ambient conditions where the Raman measurements are conducted. Te, a period six element, is highly surface active. The introduction of Te in the system improves the chemicapillary force leading to the generation of microbumps.

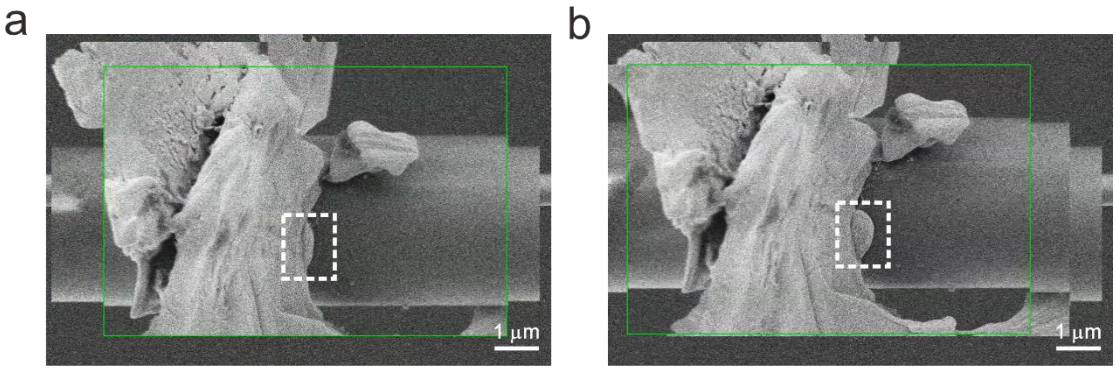

Fig. S5. The microbumps at the interface of Sb_2Te_3 plate and microfiber expands with the laser power. The white box represents the observed micropump. The average power is (a) 0.17 mW and (b) 0.32 mW.

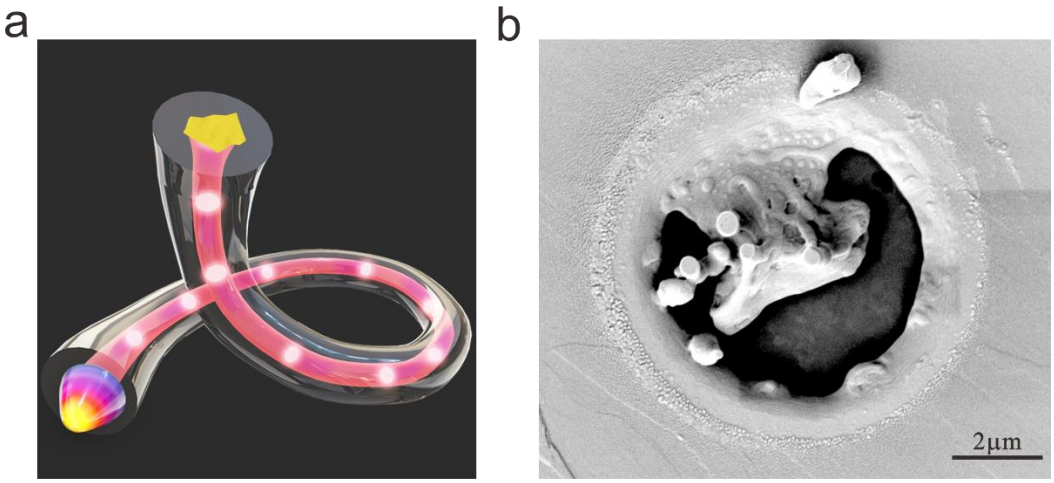

Fig. S6. Observation of thermal effects on a Sb_2Te_3 plate put on a standard fiber face. (a) Sketch of the experimental setup. A Sb_2Te_3 plate is transferred onto a fiber endface (SMF-28, from Corning Company). The fiber core and the plate overlap each other well. Nanosecond laser pulses are guided through the fiber and impinges on the plate. (b) SEM image of the plate after irradiated by nanosecond laser pulses. Around the center of the plate, a hole is formed by laser ablation, and a few microbumps are induced due to the Marangoni effects. A myriad of small spheres is produced in the cold peripheral region due to dewetting effects.

Supplementary Note 1. Simulations of Temperature Distribution in Sb_2Te_3 Plates

In a Sb_2Te_3 plate and microfiber hybrid system such as the one studied in Fig. 1(e) in the main text, the transient temperature evolution of the Sb_2Te_3 plate is calculated by the heat conduction equation

$$C_p\rho\frac{\partial T(\boldsymbol{r},t)}{\partial t}+\nabla\cdot(k\nabla\mathrm{T}(\boldsymbol{r},t))=Q_d(\boldsymbol{r},t) \tag{S1}$$

where C_p, ρ and k are the thermal capacity, density and thermal conductivity of Sb_2Te_3, respectively. COMSOL Multiphysics software is used to solve this equation and the reference temperature is 293.15 K. In the calculation, the thermal parameters

used in the numerical simulations are listed in table S1

	Specific heat capacity c_p [J/(kg · K)]	**Thermal conductivity** k [W/(m · K)]	**Density** ρ [kg/m^3]
Sb_2Te_3	205.5	2.5	6500
Au	120	310	19300
SiO_2	730	1.4	2200

Table S1. Thermal parameters used in the numerical simulations.

$Q_d(\boldsymbol{r}, t)$ is the heat power volume density of the nanosecond light pulse, with a unit of $\mathrm{W/m^3}$. $Q_d(\boldsymbol{r}, t)$, which exists in the Sb_2Te_3 plate, is set as follows

$$Q_d(\boldsymbol{r}, t) = W \frac{1}{\sqrt{\pi}\tau} \exp\left[-\frac{(t-t_0)^2}{\tau^2}\right] \frac{1}{\sqrt{\pi} S_x} \exp\left[-\frac{(x-x_0)^2}{{s_x}^2}\right] \qquad \text{(S2)}$$

where t_0 and τ denote the time delay of the pulse peak and the half temporal width of the pulse, respectively, x_0 and s_x denote the *x*-coordinate center and the half spatial width along the x-axis of the absorbed power, and W is the total absorption energy under illumination of a single pulse. For Sb_2Te_3 and Au studied in Fig. 1(e) in the main text, we take W=0.5, 5 nJ, respectively.

Supplementary Note 2. Liquid-like Motion of Sb_2Te_3 Plates Driven by Asymmetric Deformations of Microbumps

We analyze the liquid-like motion demonstrated in Fig. 6 in the main text by referring to Fig. S7. The net tension at two ending points on the contact line between the microbump and the microfiber (A and B points, see Fig. S7) is given by the Young's equation as below

$$t_A = \gamma_S^A - \gamma_{SL}^A - \gamma_L^A cos\theta_A$$

$$t_B = \gamma_S^B - \gamma_{SL}^B - \gamma_L^B cos\theta_B$$

where γ_S^A (γ_S^B), γ_{SL}^A (γ_{SL}^B), and γ_L^A (γ_L^B) are the surface tension of solid, liquid-solid interface and liquid at point A (B), respectively; $\theta_{A,B}$ denotes the contact angles. Accordingly, the tension difference between *A* and *B* points is given as

$$\Delta t = t_A - t_B = (\gamma_S^A - \gamma_S^B) - (\gamma_{SL}^A - \gamma_{SL}^B) - (\gamma_L^A cos\theta_A - \gamma_L^B cos\theta_B)$$

Assuming that $\gamma_S^A = \gamma_S^B$, $\gamma_{SL}^A = \gamma_{SL}^B$, $\gamma_L^A = \gamma_L^B$. When the microbump is at equilibrium state with $\theta_A = \theta_B$ (Fig. S7a), the tension difference Δt is equal to zero. While the equilibrium state is broken with $\theta_A \neq \theta_B$ (Fig. S7(b)), we have $\Delta t \neq 0$. For instance, considering $\theta_A > \theta_B$ as demonstrated in Fig. 6b in the main text, there is $\Delta t > 0$.

Accordingly, the microbump translates towards the left side, thereby explain the observations in Fig. 6(a).

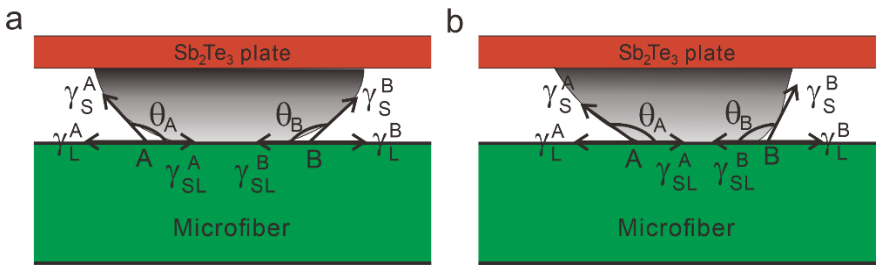

Figure S7. Sketch of cross sections of a sombrero-shaped microbump. The microbump is in equilibrium state (a) and non-equilibrium state (b).